Physics with Sub-GeV Neutrino Beams

Fritz DeJongh and Panagiotis Spentzouris
Fermilab

1 Introduction

Recently, a machine study for a new proton driver at Fermilab has been completed [1]. This proton driver would provide a front-end for a muon storage ring based neutrino factory [2] for which the physics potential has been documented in Ref. [3]. This proton driver could also provide for higher intensity conventional neutrino beams. Two new neutrino experiments which will use conventional neutrino beams are currently under construction at Fermilab: MiniBooNE and MINOS. The MiniBooNE beamline uses primary protons from the FNAL Booster (8 GeV energy) and produces a neutrino spectrum with a broad energy range from 0 to 2 GeV. The MINOS beamline uses primary protons from the FNAL Main Injector (120 GeV energy) and there are three configurations of the beamline resulting in neutrino spectra in the multi-GeV range. An upgraded FNAL proton driver could significantly increase the performance of these (or similar) beamlines. For beams created by protons from the Main Injector, intensity increases of a factor of four over NuMI are possible. The physics potential of such beams has been discussed in Ref. [4]. For beams created by protons directly from the proton driver, intensities a factor of 20 times that of MiniBooNE are possible. We discuss the physics potential of such beams in this report, focusing on measurements of $\nu_\mu \to \nu_e$ oscillations.

The neutrino oscillation probability is a function of L/E, where the baseline L is the distance from the neutrino source to the detector, and E is the neutrino energy. A conventional neutrino beam is created by focusing charged pions and letting them decay: $\pi \to \mu\nu$. The neutrino flux in the forward direction from a single pion decay is also a function of L/E [4]. Thus, for a given oscillation probability, the neutrino flux per pion decay is independant of energy. Though to a very good approximation neutrino cross-sections are linear with neutrino energy, there are several reasons that lower energy beams may still be competitive:

1. The main injector limits the possible increase in proton intensity for a MINOS-type beam, while a BooNE-type beam could, in principle, use the full intensity of a new proton driver.

2. Pion production peaks at low energy, which results in a greater production of low-energy neutrinos.

3. The intrinsic ν_e component of the beam is smaller at lower energies, resulting in a lower background for a ν_e appearance signal.

4. At low energies, a water or mineral oil Cerenkov ring detector is very suitable for detecting the electron signal and rejecting the muon and π^0 backgrounds. At higher

energies, a more expensive and less mature detector technology would be needed. Since very high mass detectors are required in order to enhance the physics reach of next generation conventional beam experiments [4], low energy beams have the advantage of providing more detector mass per dollar spent.

We also note that the lower energy beamlines are cheaper and faster to build, so there is a better chance a neutrino experiment would be ready by the time the new proton driver is built. This is of course true if the power of the proton driver is in the 1MW range [5]. For higher output of the proton driver, the design of the target and focusing system is more challenging. In this case, such a design is very similar to that of the front-end of a neutrino factory; thus the R&D effort could be shared with that for a neutrino factory. The tapered solenoids envsioned for collecting pions for a neutrino factory can produce a very suitable conventional neutrino beam, except that additional components will need to be designed to separate π^+ from π^- [6]. In any case, since the target and pion decay tunnel for a low energy beamline are similar to the front-end of a neutrino factory, it might be possible to design such a beamline to also provide a muon beam for muon cooling R&D. Thus, a low energy beamline may be a better fit to a long-range neutrino physics program culminating in a neutrino factory.

2 Theoretical Summary

The matter-antimatter asymmetry of the universe implies CP violation in particle interactions. CP violation in the standard model is not able to explain this asymmetry. Studies of CP violation in the lepton sector may provide some insight into this question, and may involve unexpected phenomena. For example, the existence of eV-scale sterile neutrinos would require a dramatic extension of the standard model, and there could be large CP asymmetries in the oscillations to these neutrinos. Hence, one of the most important objectives for the next generation neutrino experiments would be to search for CP violation effects in the neutrino sector. Another objective would be the high accuracy determination of all the parameters of the neutrino mixing matrix.

Neutrino oscillation models with three generations of neutrinos are able to explain two out of three possible oscillation frequencies. The usual choice for three generation scenarios is to incorporate the solar and atmospheric neutrino deficits. To explain the LSND effect as well, one or more generations of sterile neutrinos is needed. These models are summarized in Fig. 1

In the three generation model, oscillations between ν_e and ν_μ explain the solar neutrino deficit. Such oscillations can also occur at the atmospheric frequency via the component of the third mass eigenstate in the ν_e and ν_μ flavor eigenstates. At short baselines, neglecting the solar oscillations, (the "leading" approximation), we have:

$$P(\nu_\mu \to \nu_e) = \sin^2\theta_{23}\ \sin^2 2\theta_{13}\ \sin^2\left(1.267\ \Delta M^2_{23}\ \frac{L}{E}\right) \tag{1}$$

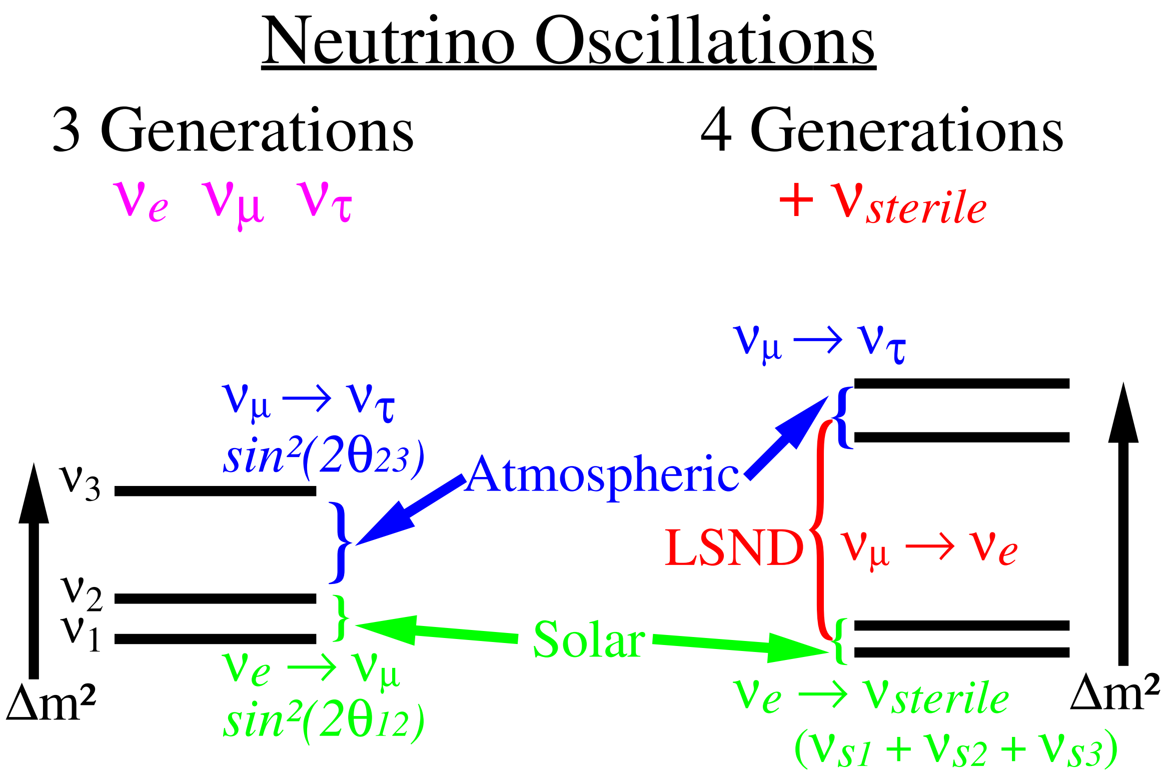

Figure 1: Overview of neutrino oscillation models.

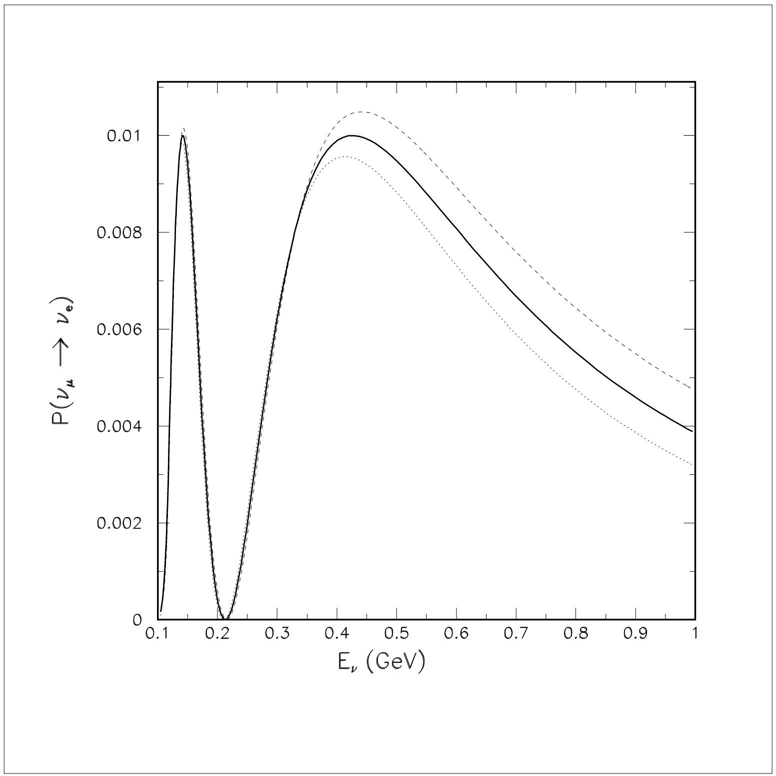

Figure 2: Matter effects and the oscillation probability, for L=150 km. Solid line: vacuum. Dashed line: neutrinos in Earth's crust. Dotted line: anti-neutrinos in Earth's crust.

with ΔM^2_{23} in eV^2, L in km, and E in GeV. Thus, a ν_e appearance experiment in a conventional ν_μ beam can determine $\sin^2 2\theta_{13}$. Matter effects can modify these oscillations, and make the measurement sensitive to the sign of ΔM^2_{23}. However, these effects are small for the energies considered here and we neglect them in this report. However, as illustrated in Fig. 2, there still is a possibility of observing these matter effects if enough events are observed.

When considering the solar oscillations, interference between the atmospheric and solar oscillations generates CP-odd terms and can lead to observable CP asymmetries in the case of the Large-Mixing-Angle (LMA) solution to the solar neutrino deficit. The CP asymmetry is modulated at the solar frequency. With low energy beams in the LMA scenario, these effects could be studied at the atmospheric baseline. The possible size of the CP-asymmetry is shown in Fig. 3.

In four generation models, leading oscillations between ν_e and ν_μ occur at the LSND baseline, which is much shorter than the atmospheric baseline. Subleading effects occur at the atmosperic frequency, with an amplitude of the same order as the LSND amplitude. At the maximum of the atmospheric oscillation, CP asymmetries as high as nearly 100% are possible from the interference between the two types of oscillations [8].

Thus, in both types of scenario for the neutrino spectrum, an experiment to study ν_e

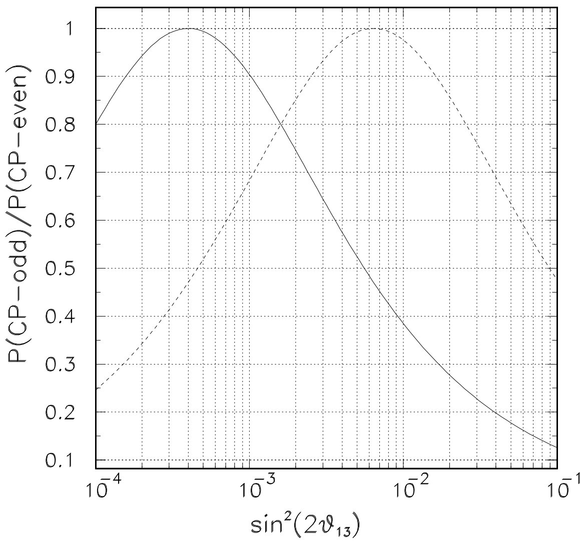

Figure 3: Ratio of CP-odd to CP-even terms in the oscillation probability, as a function of $\sin^2(2\theta_{13})$, evaluated at the maximum of the atmospheric oscillation, for maximal CP violation. We assume $\Delta M^2_{12}/\Delta M^2_{23} = 0.014$ (solid line), $\Delta M^2_{12}/\Delta M^2_{23} = 0.056$ (dashed line), $\sin^2(2\theta_{12}) = 0.8$, and $\sin^2(2\theta_{23}) = 1$.

appearance in a ν_μ beam, at atmospheric baselines, is well motivated.

3 Simulation tools and detection assumptions

For this project, we have used the MiniBooNE simulation. This includes a Geant simulation of the target and beamline. For each hadron that produces a neutrino, another program simulates a decay as many times as desired. Finally, another program generates the final state particles for each type of neutrino reaction, and assigns a weight for each type of reaction. Although we have been using neutrino cross-sections for carbon, we are assuming they will be similar for oxygen as well.

We estimate the visible energy for an event from the energy of electrons, π^0, and muon energy above cerenkov threshold.

The results in this report assume only one horn. The MiniBooNE simulation includes the option of a second horn, which we will investigate in the future. Other options we will explore are the use of plugs, dipoles, and hadronic hoses to optimize the spectrum.

Based on the MiniBooNE TDR, for electron reconstruction efficiencies, we assume 50%. We assume a rejection of 0.01 for π^0, and 0.001 for muons. This is consistent with Super-K performance as well [7].

4 Spectra

The neutrino spectrum at the MiniBooNE detector has a broad distribution between 0 and 2 GeV. This is a good feature for a search for oscillations with a ΔM^2 that is not known. For the experiments we are envisioning, the atmospheric ΔM^2 will be well known and we can optimize the energy and baseline for the expected signal. Going to an energy below 0.6 GeV has some advantages:

1. The ν_e CC cross-section is still appreciable, while the cross-section for NC production of a π^0 is relatively suppressed. The cross-sections for the signal and the main background processes are shown in Fig. 4.

2. The π^0 rejection at low energy is more effective since the two photons from the π^0 decay have an appreciable opening angle and create separate cerenkov rings.

It is possible to obtain a softer neutrino spectrum by placing the detector at an angle relative to the beamline. This is illustrated in Fig. 5. For this report, we will choose $\cos\theta \approx 0.9985$. Fig. 6 shows the energy spectra for neutrinos at this angle.

5 Visible energy distribution

The visible energy distributions for the signal and the main backgrounds are shown in Fig. 7. For the signal process, $\nu_e C \to eN$, we take the electron energy to be the visible energy. For

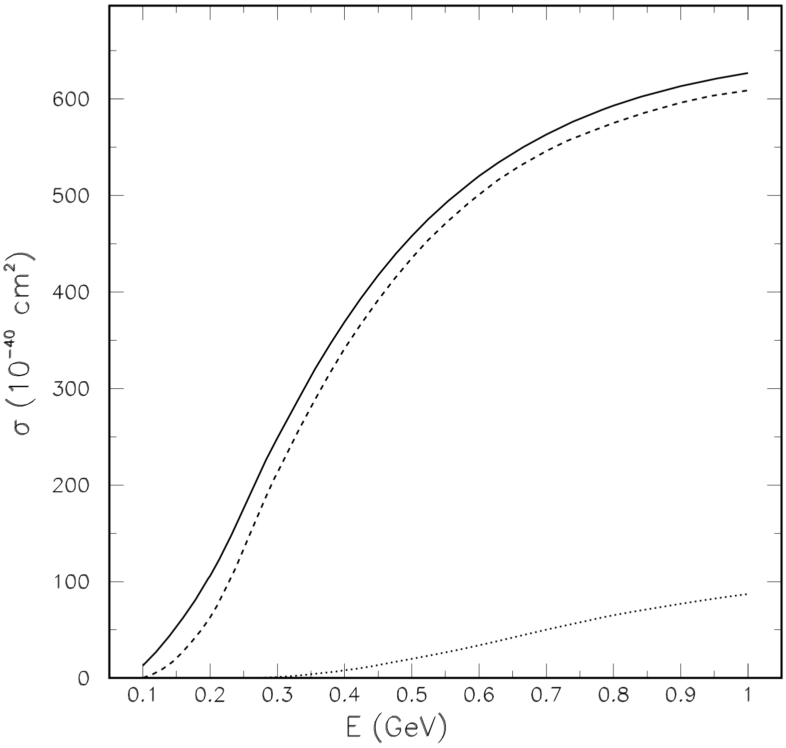

Figure 4: Solid line: Cross-section for $\nu_e C \to eN$. Dashed line: Cross-section for $\nu_\mu C \to \mu N$. Dotted line: Cross-section for $\nu C \to \nu \pi^0 X$.

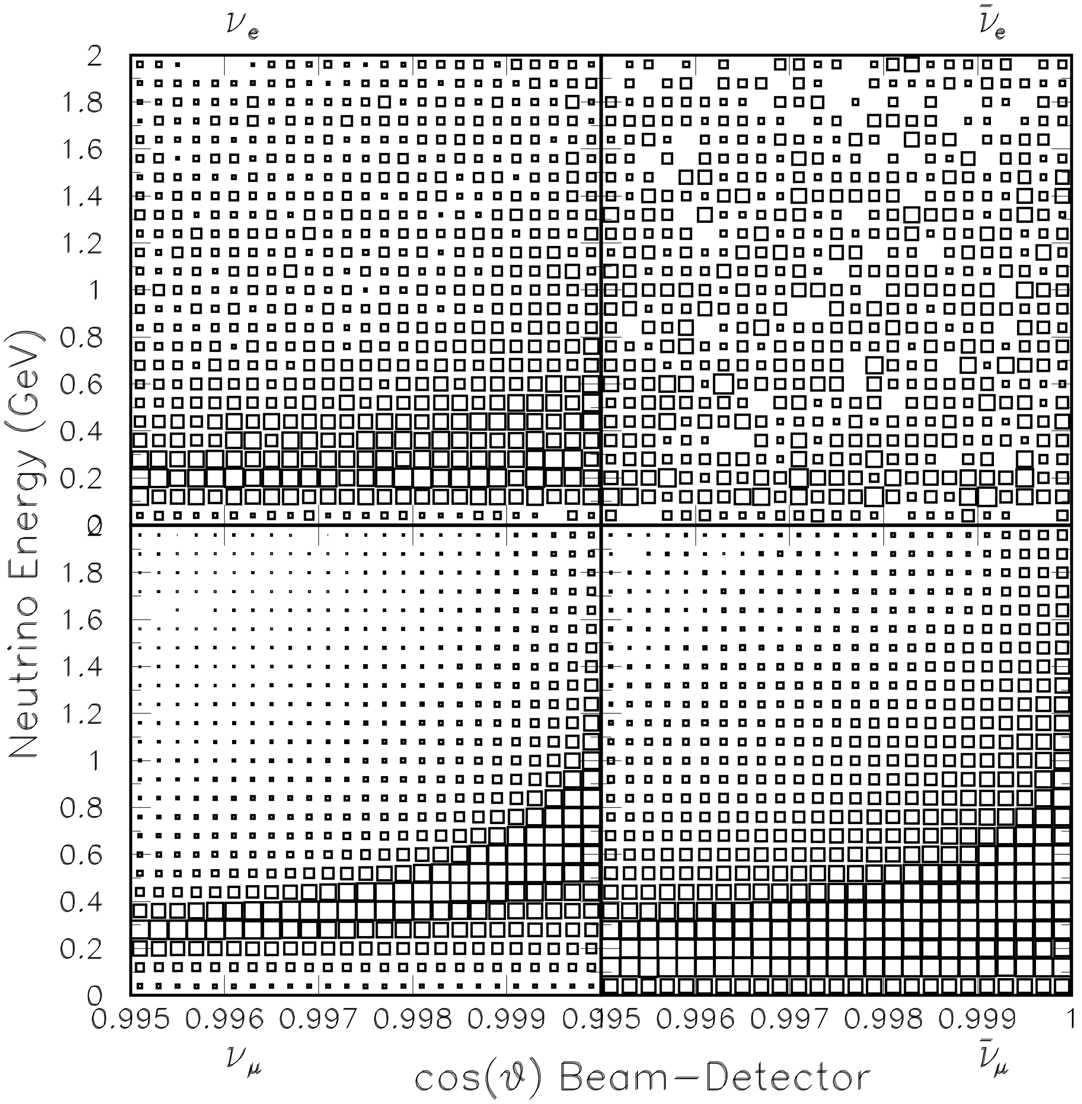

Figure 5: Neutrino energy spectrum vs. the angle between the beam and detector, for the various beam components.

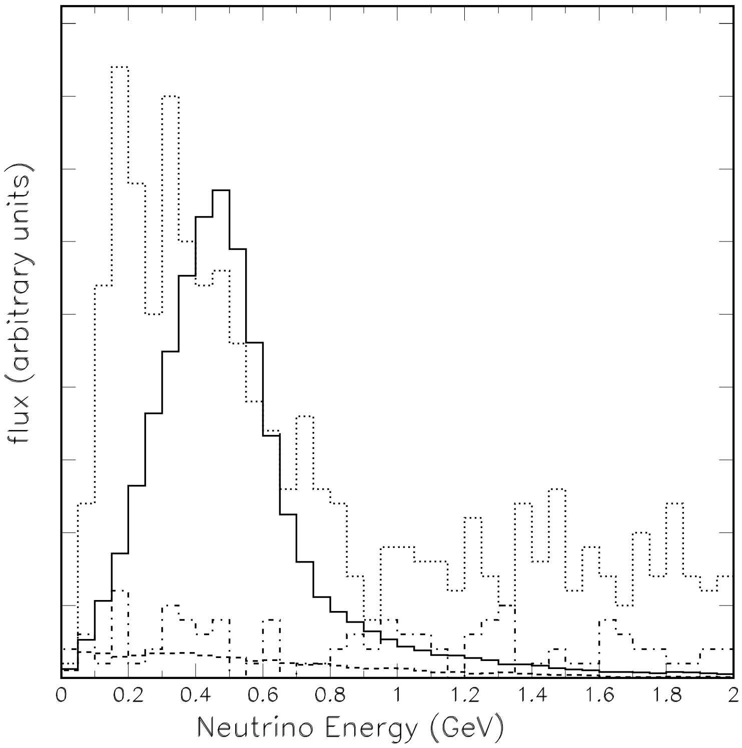

Figure 6: Neutrino energy spectrum for the different components: Solid: ν_μ. Dashed: $\bar{\nu}_\mu$. Dotted: $500\times$ ν_e. Dot-Dashed: $500\times$ $\bar{\nu}_e$.

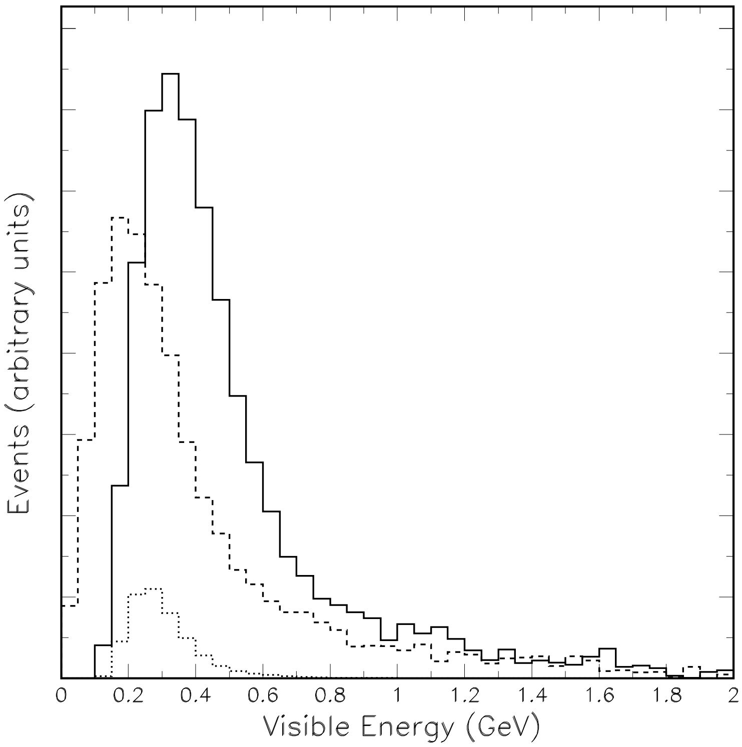

Figure 7: Visible energy distribution. Solid line: $\nu_e C \to eN$, assuming 100% $\nu_\mu \to \nu_e$. Dashed line: $\nu_\mu C \to \mu N$, assuming 100% $\nu_\mu \to \nu_\mu$. Dotted line: $\nu C \to \nu \pi^0 X$.

the background process $\nu_\mu C \to \mu N$ we take the visible energy to be the muon kinetic energy above cerenkov threshold. As a result, the visible energy distribution is shifted down relative the the signal distribution. For the background process $\nu C \to \nu \pi^0 X$, we take the visible energy distribution to be the π^0 energy.

6 Reach in $\sin^2 2\theta_{13}$.

Assuming an 8 GeV proton beam on target with a power of 0.75 MW, which seems a reasonable choice for magnetic horn technology, a water Cerenkov detector at a 150 km baseline with 1000 kt-yr exposure, $\Delta M^2 = 3.5 \times 10^{-3}$ eV^2, $\sin^2 2\theta_{13} = 0.004$, and $\sin^2 2\theta_{23} = 1.0$, we find the results in Fig. 8. There are 80 background events and 28 signal events, corresponding to a 3σ signal.

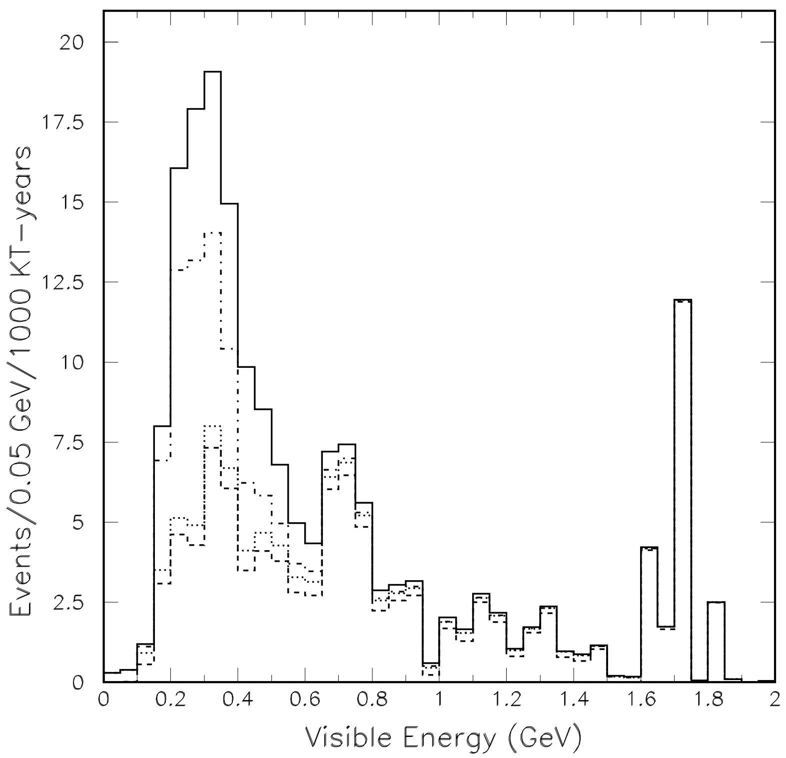

Figure 8: Solid line: Total signal + background. Dashed: Beam ν_e background. Dotted: Addition of muon background. Dot-Dashed: Addition of π^0 background.

7 Reach in CP measurements

The measurement of CP violation requires running with $\bar{\nu}$ beams as well as ν beams. We have found that the signal rate for $\bar{\nu}$ beams is reduced by a factor of seven, from a combination of a reduced π^- production rate and a smaller cross-section.

Furthermore, there are relatively more backgrounds, mainly from ν contamination in the beam. With a simplified model, we have studied the effect of placing a dipole bend after the horn, and find that it quite effectively removes this source of contamination. We therefore assume that we can obtain a $\bar{\nu}$ signal with the same signal to noise, but with seven times less rate than the ν case.

With a 0.75 MW proton beam, CP violation can be detected only in the four-generation model, and only if there is a relatively large $\bar{\nu}_\mu \to \bar{\nu}_e$ probability, of order 0.02, with a much smaller probability for $\nu_\mu \to \nu_e$. To improve the sensitivity with the same detector, an upgrade to a 4 MW proton driver would be necessary. In this case, maximal CP violation in the 3-generation model could be detected at the 3σ level for large values of $\sin^2 2\theta_{13}$, if $\Delta M^2_{12} > 7 \times 10^{-5}$ eV^2. In the absence of background, the statistical sensitivity to CP violation is independant of $\sin^2 2\theta_{13}$ as long as the leading terms are larger than the sub-leading terms. Therefore, the sensitivity to CP violation for small values of $\sin^2 2\theta_{13}$ will depend on background levels. Fig. 9 shows, for the background levels in Fig. 8, the minimum value of ΔM^2_{12} allowing a 3σ observation of maximal CP violation, as a function of $\sin^2 2\theta_{13}$.

8 Conclusions

The most critical issue currently facing the neutrino physics community is whether neutrino oscillations are needed to explain the LSND effect. The MiniBooNE experiment will resolve this question, and the outcome will in general have a major impact on planning for future experiments. So, it is interesting that the measurement of $\nu_\mu \to \nu_e$ oscillations at the atmospheric baseline is important in either scenario.

We have investigated the option of studying $\nu_\mu \to \nu_e$ oscillations with a low energy neutrino beam similar to that of MiniBooNE, but generated using a 0.75 MW proton beam. We have used the MiniBooNE tools to obtain signal and background rates. We have found that placing the detector off of the beam axis produces a low-energy spectrum with very good background properties. The target and decay tunnel for such a beam can more easily be part of a stage of a neutrino factory than is the case for higher-energy superbeams.

With a large water cerenkov detector, such as for the UNO proposal [9], we find a reach in $\sin^2 2\theta_{13}$ of 0.004, comparable to the higher-energy superbeam proposals. Since the signal rate in $\bar{\nu}$ beams is very low, we find that an upgrade to a 4 MW proton driver may be necessary to start studying CP violation.

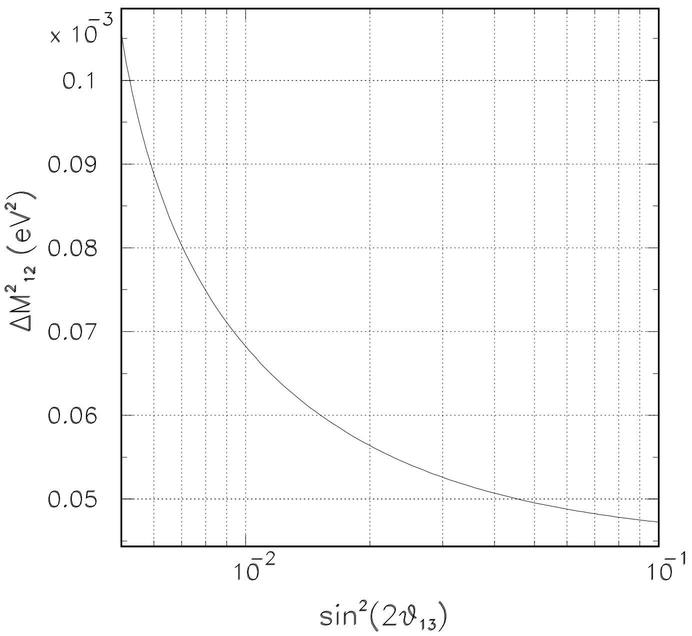

Figure 9: For the background levels in Fig. 8, the minimum value of ΔM^2_{12} allowing a 3σ observation of maximal CP violation, as a function of $\sin^2 2\theta_{13}$.

References

[1] R. Alber *et al.*, fermilab-tm-2136, http://www-bd.fnal.gov/pdriver/reports.html

[2] T. Anderson *et al.*,
http://www.fnal.gov/projects/muon_collider/nu/study/report/machine_report/

[3] C. Albright *et al.*, fermilab-fn-692, hep-ex/0008064

[4] V. Barger *et al.*, fermilab-fn-703, hep-ex/0103052

[5] For the MiniBooNE horn and target design (see MiniBooNE beamline TM), assuming 5×10^{12} protons per pulse at 7.5 Hz, the heat power from the beam is ~ 0.3 of that due to the current pulse on the horn. Taking this number as a guidline, and ignoring radiation, shielding and other such effects, it seems reasonable to assume that a similar horn and target design could operate at 1 MW proton source power.

[6] We thank Nikolai Mokhov for producing files for an initial look at this issue.

[7] Dave Casper, private communication.

[8] K. Dick, M. Freund, M. Lindner and A. Romanino, Nucl. Phys. B **562**, 29 (1999) [hep-ph/9903308].

[9] C. K. Jung, hep-ex/0005046.